Proceedings of ASME Turbo Expo 2013
GT2013
June 3-7, 2013, San Antonio, Texas, USA

GT2013-94034

TURBOCHARGER SYNCHRONOUS VIBRATION CONTROL ON HIGH SPEED BALANCER. TEST AND PREDICTION

Kostandin GJIKA*, Antoine COSTEUX
Honeywell Turbo Technologies,
Zone Industrielle Inova 3000,
2 Rue de l'Avenir,
88155 Thaon-les-Vosges, France
email: kostandin.gjika@honeywell.com,
antoine.costeux@honeywell.com

Pradeep MAHADEVAN
Honeywell Technology Solutions Lab,
151/1, Doraisanipalya,
Bannerghatta Road,
Bangalore-560076, India
email: pradeep.mahadevan@honeywell.com

ABSTRACT

Current trends for advanced automotive engines focusing on downsizing, better fuel efficiency and lower emissions have led to several changes in turbocharger bearing systems design and technology. Automotive turbochargers are running faster under high engine vibration level. Vibration control is becoming a real critical issue and turbocharger manufacturers are focusing more and more on new and improved balancing technology.

This paper deals with turbocharger synchronous vibration control on high speed balancers. In a first step the synchronous rotordynamics behavior is identified. The developed fluid bearing code predicts bearing rotational speed (in case of fully-floating design), operating inner and outer bearing film clearances and bearing force coefficients. A rotordynamics code uses this input to predict the synchronous lateral dynamic response of the rotor-bearing system by converging with bearing eccentricity ratio. The rotor-bearing system model is validated by shaft motion test data on high speed balancer (HSB). It shows that only one of the peaks seen on the synchronous G level plot collected in a high speed balancer can be explained by rotordynamics physics. A step-by-step structural dynamics model and analysis validated by experimental frequency response functions provides robust explanations for the other G level peaks. The synchronous vibration response of the system "turbocharger-HSB fixture" is predicted by integrating the predicted rotordynamics rotational bearing loads on the structural dynamics model. Numerous test data show very good correlation with the prediction, which validates the developed analytical model.

The "rotordynamics – structural dynamics model" allows deep understanding of turbocharger synchronous vibration control as well as optimization of the high speed balancer tooling.

INTRODUCTION

Foundation flexibility in turbomachinery affects the rotor-bearing system (RBS) behavior. The inclusion of foundation characteristics in a RBS model has been the focus of many research studies [1-6]. Cavalca et al. [7] investigated the influence of flexible versus rigid foundation structure on RBS forced response. They modeled the rotor-bearing and foundation using finite element modeling (FEM) and reduced the number of foundation degrees of freedom (DOF) using a modal analysis approach on measured frequency response functions (FRFs). Cavalca et al. concluded that in large rotors, foundation flexibility affects significantly the rotor-bearing unbalance response. Xu and Vance [2] identified critical speeds in RBS due to foundation flexibility. Hence, it is essential to include foundation characteristics in a RBS model in order to accurately predict the system forced response.

Representing the foundation characteristics using measured FRFs provides relatively a fast and accurate solution. Modal analysis consists of three stages: FRF measurements, foundation parameter identification, and implementation of the identified modal parameters in a mathematical or numerical model [8].

FRFs can be obtained analytically (using FEM programs i.e. ANSYS, NASTRAN) or experimentally. Obtaining accurate FRF measurements is a key step for a valid modal analysis. Yamaguchi [9] introduced an advanced new method, making best use of FFTs (Fast Fourier Transformation) in FRF

*Corresponding author

measurements. In addition, Ewins [8] provided extensive guidelines regarding FRF measurement techniques.

In prior studies, Xu and Vance [2] followed the method developed by Nicholas et al. [1] to calculate bearing equivalent coefficients consisting of the true bearing force coefficients and foundation modal parameters (extracted from measured or analytically derived FRFs). In both cases, [1] and [2] the bearing equivalent coefficients consisted of only direct terms. In other words, the cross-coupled effects among FRF measurement locations on the foundation were not considered. In addition, both analyses required extraction of modal parameters from foundation FRFs. Nelson [10] provided the first commercially available rotordynamics code (ARDS) to include foundation modeling with FRF data.

The full FEM of the turbomachinery that includes rotor-bearing system and housings is also another alternative for forced vibration prediction. Sometimes, this approach can be costly and time consuming for complex and nonlinear behavior foundation structures.

In this paper an original approach for synchronous forced response prediction on the housing of a turbocharger is developed and validated by test data. This includes three steps: bearing loads calculation by a rotordynamics prediction code, structural dynamics modeling of housings and harmonic analysis that combines the first two steps for prediction of forced vibration on the housing. It is successfully applied for the vibration prediction of an automotive turbocharger on high speed balancer.

AUTOMOTIVE TURBOCHARGERS DESCRIPTION

Actual turbochargers are using conventional bearing technologies like fluid film bearings [11] or ball bearings [12], and advanced technologies such as oil-less bearing [13] are under investigation.

Figure 1 presents a fully-floating hydrodynamic bearing turbocharger. The floating ring bearings consist of two bushings which have a clearance fit between both the shaft and housing so that two hydrodynamic oil films are created as the shaft (and therefore the unbalance load vector) rotates. Such design provides relatively high damping performance for reduced transmissibility and controlled rotor deflection of the rotating group. The axial load is supported by a separated hydrodynamic thrust bearing. It is the original and low cost rotor-bearing system design used on both light vehicle (LV) and commercial vehicle (CV) applications, but more susceptible to shaft motion instability due to two hydrodynamic oil films (inner and outer); relatively difficult to be balanced over a high speed range of turbocharger when the design integrates a rigid shaft. Recently both synchronous & subsynchronous vibrations have become an issue on vehicle.

Figure 2 shows a recent semi-floating hydrodynamic bearing turbocharger. The bearing system consists of a single bushing with two bearing radial lands and integrated hydrodynamic thrust bearing; the inner shape of radial bearing has 4 axial groves. The bushing is prevented from rotating by a pin, the inner oil film operates then as a hydrodynamic bearing and the outer film acts as a pure squeeze film damper. Such a design allows: reduced journal diameter and radial power losses; relatively high damping provided by squeeze film damper; very good shaft motion stability, even under low oil viscosity and high oil inlet temperature; low transmissibility due to the use of a flexible shaft (slender shaft) and low initial unbalance due to rotating group design concept; a less rich subsynchronous frequency content compared to fully-floating bearing, and consequently less problems with the respect of noise issues; an easy design for overall bearing system performance optimization. It is successfully used on LV applications.

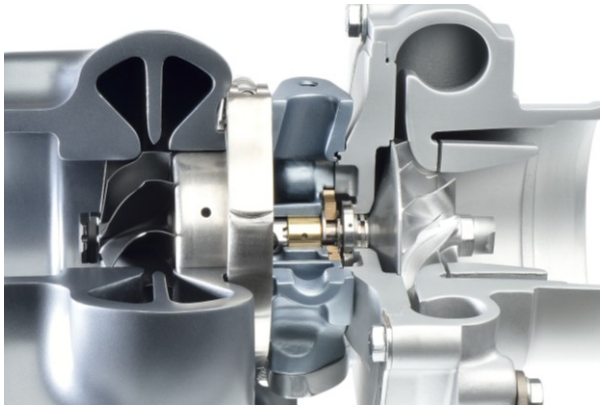

Figure 1. FULLY-FLOATING HYDRODYNAMIC ROTOR-BEARING SYSTEM

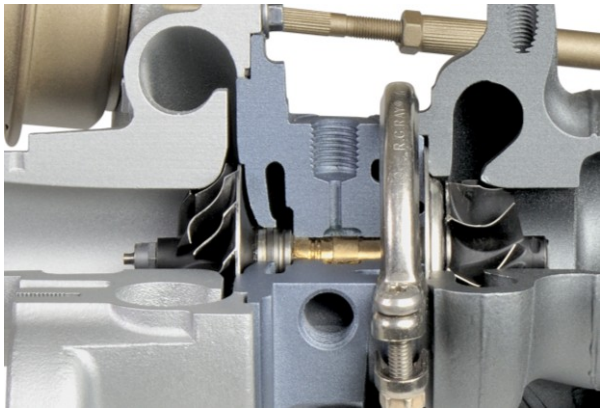

Figure 2. SEMI-FLOATING HYDRODYNAMIC ROTOR-BEARING SYSTEM

Figure 3 describes a ball bearing turbocharger recently in production for both LV and CV applications. The inner race of ball bearing cartridge is press fitted on the shaft, the outer race is blocked in rotation by an antirotation pin and the outer oil film operates as squeeze film damper. It is a demonstrated design for transient performances with very low power losses

and exceptional cold start [12]; very good shaft motion dynamic stability due to the lack of hydrodynamic oil film; subsynchronous vibration is not an issue; relatively difficult to be balanced due to increased rotating group rigidity and consequently large dynamic bearing loads; oil contamination can be an issue for rotor-bearing system and relatively high cost design.

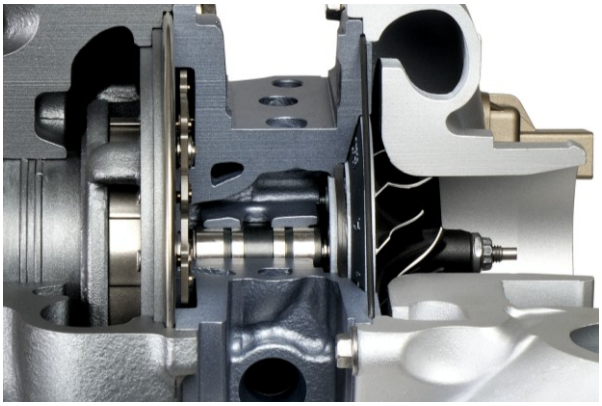

Figure 3. BALL BEARING ROTOR-BEARING SYSTEM

In reference [13] a turbocharger with hydrodynamic foil bearings is presented. The perceived benefits are lower emissions, packaging flexibility, simpler installation, lower vibration transmissibility and improved reliability.
In this paper the application concerns a hydrodynamic semi-floating bearing system turbocharger.

A FORCE RESPONSE METHOD FOR SYNCHRONOUS VIBRATION PREDICTION

A step by step approach for synchronous forced response prediction on housings of a turbocharger is developed and validated by test data. This includes three steps: bearing loads calculation by a rotordynamics prediction code, structural dynamics modeling of housings, and harmonic analysis that combines the first two steps prediction of forced vibration.

Primer on synchronous rotordynamics behavior

Theoretical aspects employed for rotor-bearing system lateral dynamics modeling and associated finite element code are described by Childs in [14].

The differential equation of the linear dynamic behavior of a rotor-bearing system under external synchronous excitation forces can be written:

$$[M]\{\ddot{\delta}\}+[C]\{\dot{\delta}\}+\Omega[G]\{\dot{\delta}\}+[K]\{\delta\}=\{F_{ext}(\Omega t)\} \quad (1)$$

where:

$\{\delta\}$, nodal displacement vector contains all the real DOF (translations and rotations) of the system in a global reference frame
$[M]$, mass matrix including shaft, discs and bearing inertia characteristics
$[C]$, damping matrix including shaft and bearing
$[G]$, gyroscopic matrix
$[K]$, stiffness matrix including shaft and bearing
$\{F_{ext}(\Omega t)\}$, external synchronous excitation forces vector

The finite element formulation uses Timoshenko beam theory [15] and implements component-mode synthesis [16] in order to model multiple shaft rotors. The mass of oil film is ignored and the force coefficients (oil stiffness and damping coefficients) are valid only for small amplitude motions or perturbations around a dynamic equilibrium.

The damped natural frequencies of rotor-bearing system can be defined by solving the homogeneous form of the equation (1):

$$[M]\{\ddot{\delta}\}+[C]\{\dot{\delta}\}+\Omega[G]\{\dot{\delta}\}+[K]\{\delta\}=\{0\} \quad (2)$$

Assuming $\{\delta\}=\{d\}e^{rt}$ on the equation (2) and solving the associated characteristics equation:

$$\left[r^2[M]+r[C]+r\Omega[G]+[K]\right]\{d\}=\{0\} \quad (3)$$

leads to a problem of eigenvalues $r=(\lambda + i\omega)$ and eigenvectors $\{d\}$, also known as natural damped mode shapes. Dynamic stability of a linear dynamic behavior system requests that the real part, λ, of all eigenvalues to be negative.

The system response under unbalance forces $\{F_{ext}(\Omega t)\}=m\{\delta\}\Omega^2 e^{i\Omega t}$ can be written $\{\delta\}=\{\Delta\}e^{i\Omega t}$ and determined by solving the following algebraic equation:

$$\left[-\Omega^2[M]+i\Omega[C]+i\Omega^2[G]+[K]\right]\{\Delta\}=m\{\delta\}\Omega^2 \quad (4)$$

Summary of fluid film bearing analysis

Gjika and LaRue [17] detailed the physical model and computational analysis for prediction of the forced performance of fluid film radial bearings.
Starting with the Navier-Stokes and continuity equations for a fluid element, the hydrodynamic film bearing equation can be derived from Osborne Reynolds approach detailed on [18]. For an incompressible fluid and steady state loading, the equation is:

$$\frac{\partial}{\partial x}\left(\frac{h^3}{\mu}\frac{\partial p}{\partial x}\right)+\frac{\partial}{\partial z}\left(\frac{h^3}{\mu}\frac{\partial p}{\partial z}\right)=6U\frac{\partial h}{\partial x} \qquad (5)$$

where:

h,	film thickness
μ,	fluid viscosity
p,	fluid pressure
x and z,	dimensions
U,	journal surface speed.

Assuming the bearing is infinitely short (the length-to-diameter ratio of most turbocharger bearings is about 0.5), the short bearing theory can be used to model the oil films of both the fully-floating and semi-floating bearings. The film pressure decreases more rapidly axially than circumferentially and the pressure derivative in the circumferential (i.e., x) direction can be set to zero, figure 4.

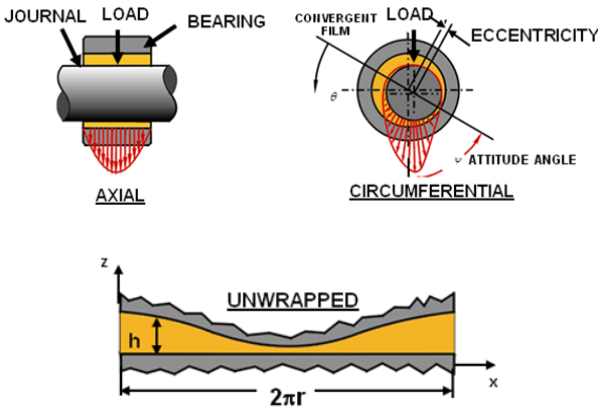

Figure 4. RADIAL AND AXIAL PRESSURE DISTRIBUTION ON HYDRODYNAMIC BEARING

That leads to the simplified equation (6):

$$\frac{\partial}{\partial z}\left(\frac{h^3}{\mu}\frac{\partial p}{\partial z}\right)=6U\frac{\partial h}{\partial x} \qquad (6)$$

If the film thickness is only a function of circumferential dimension, x, and by setting the film pressure equal to zero at each end of the bearing, the integration of the equation (6) gives:

$$p(\theta,z)=\frac{3\mu U}{Rc_r{}^2}\left(\frac{L^2}{4}-z^2\right)\frac{\varepsilon\sin\theta}{(1+\varepsilon\cos\theta)^3} \qquad (7)$$

where:

θ,	angular location
R,	journal radius
L,	bearing length
ε,	eccentricity ratio ($\varepsilon = e/c_r$, e - journal eccentricity and c_r - radial bearing clearance).

The oil film pressure is modeled only for 180° of the bearing arc and the remaining arc is set to ambient pressure - cavitated π film model. This allows defining the two following orthogonal forces:

$$W_x=\frac{\mu UL^3}{c_r{}^2}\frac{\varepsilon^2}{(1-\varepsilon^2)^2} \qquad (8)$$

$$W_y=\frac{\mu UL^3}{4c_r{}^2}\frac{\pi\varepsilon}{(1-\varepsilon^2)^{1.5}}$$

where:

W_x,	the force in the direction of the applied load
W_y,	the force at the right angle of the applied load

The total load can then be computed:

$$W=\frac{\mu UL^3}{4c_r{}^2}\frac{\varepsilon}{(1-\varepsilon^2)^2}\left[\pi^2(1-\varepsilon^2)+16\varepsilon^2\right]^{0.5} \qquad (9)$$

The load capacity number, Λ, can be now calculated:

$$\Lambda=\frac{\mu DL^3N_{eff}}{60Wc_r{}^2}=\frac{\left(1-\varepsilon^2\right)^2}{\pi\varepsilon\left[\pi^2\left(1-\varepsilon^2\right)+16\varepsilon^2\right]^{0.5}} \qquad (10)$$

where N_{eff} is the effective speed concept developed by Stone and Underwood [19]:

$$N_{eff}=\left|2N_L-N_J\right| \qquad (11)$$

with:

N_L,	load speed
N_J,	journal speed

By assuming a load, *W*, and knowing the bearing dimensions and operating conditions, the eccentricity ratio of the bearing films can be calculated. In addition, the two films can be coupled together by assuming that both films carry the same load (i.e., the bearings are massless).

Heat transfer through the bushing is calculated between the inner (typically hotter) film and the outer film. An iteration scheme is used to converge on the mean lubricant temperature: the heat generated by shearing of the lubricant in the inner film is carried away by the calculated lubricant flow and the heat transfer to the outer film. Likewise, the calculated flow through the outer film carries away the heat generated by shearing in the outer film, plus the additional heat transferred from the inner film. Iteration continues until the assumed mean lubricant temperatures converge. The inner and outer lubricant viscosities are based on their respective mean film temperatures and are updated as the iteration proceeds. This approach is similar to that described in [20].

For the semi-floating bearing, the bearing speed is fixed at zero. For the case of the fully-floating bearing, an additional iteration loop is used to calculate bearing speed from a balance of the inner and outer film torques.

The stiffness, *K,* and damping, *B,* coefficients can be derived from equations (8):

$$K = \frac{\pi \mu R L^3 N_{eff}}{30 {c_r}^3} \left(\frac{\varepsilon}{\left(1-\varepsilon^2\right)^2} \right) \tag{12}$$

$$B = \frac{\pi \mu R L^3 N_{eff}}{4 {c_r}^3 N_S} \left(\frac{1}{\left(1-\varepsilon^2\right)^{1.5}} \right) \tag{13}$$

Using the effective speeds, the inner and outer film stiffness and damping coefficients can be computed for use in the rotordynamics modeling.

An analytical approach for synchronous forced vibration prediction

A full-modeling approach for forced vibration response prediction on turbocharger housings requires modeling aspects of the dynamic behavior of the static support structures. Several modeling techniques and numerical methods exist to predict dynamic behavior of linear or nonlinear structures. [21], [22], [23]. This paper doesn't concern the development of any new modeling techniques or numerical methods. Using a commercial prediction code [24] some specific FE models are developed for the dynamic behavior prediction of the assembly "CHRA (center housing rotating assembly) non rotating structure-HSB supporting structure". This topic is described later.

The excitation forces that act on the turbocharger housing are synchronous bearing loads due to mass unbalances on the rotating group. These forces are outputs of a rotordynamics analysis. They are rotating loads and synchronous with the speed of the rotor. To model the rotating nature of the load, an indirect finite element method is adopted. Two dummy nodes are created: one on each center of the two bearing planes. Each dummy node is connected to the nodes on the center housing bore, lying in the same axial plane, through very stiff and massless link elements. Then the excitation force (bearing load) is applied at the dummy node as two perpendicular forces with a phase difference of 90 degrees:

$$\begin{aligned} \left(F_{brg}\right)_x &= F_{brg}\, e^{i\Omega t} \\ \left(F_{brg}\right)_y &= F_{brg}\, e^{(i\Omega t + \pi/2)} \end{aligned} \tag{14}$$

where:

F_{brg}, magnitude of bearing load
Ω, rotational speed

Generally speaking, on different bearings the load vectors are different in magnitude as well as in phase angle. This is taken into account in the analysis as follows. Assume F_{brg_1} and F_{brg_2} the loads on bearing B_1 and B_2 planes respectively, and let Φ be the phase difference between them. Then the forces on the dummy nodes in the two planes will be:

$$\begin{aligned} \left(F_{brg_1}\right)_x &= F_{brg_1}\, e^{i\Omega t} \\ \left(F_{brg_1}\right)_y &= F_{brg_1}\, e^{(i\Omega t + \pi/2)} \end{aligned} \tag{15}$$

$$\begin{aligned} \left(F_{brg_2}\right)_x &= F_{brg_2}\, e^{(i\Omega t + \Phi)} \\ \left(F_{brg_2}\right)_y &= F_{brg_2}\, e^{(i\Omega t + \pi/2 + \Phi)} \end{aligned} \tag{16}$$

Once the loads on the dummy nodes are determined, a routine harmonic analysis can be carried out at each speed of interest, by solving the following differential equation of the static structure:

$$[M_{str}]\left\{\ddot{\delta}_{str}\right\} + [C_{str}]\left\{\dot{\delta}_{str}\right\} + [K_{str}]\{\delta_{str}\} = \{F_{brg}(\Omega t)\} \tag{17}$$

where:

$\{\delta_{str}\}$, nodal displacement vector contains all real DOF

$[M_{str}]$, mass matrix

$[C_{str}]$, damping matrix

$[K_{str}]$, stiffness matrix

$\{F_{brg}(\Omega t)\}$, bearing loads calculated from (15) and (16)

TURBOCHARGER FORCED SYNCHRONOUS VIBRATION ON HIGH SPEED BALANCER. PREDICTION AND COMPARISON TO TEST DATA

The developed procedure is applied for the prediction of synchronous forced vibration response of turbocharger on a HSB. Figure 5 shows a high speed balancer, on which is installed a CHRA unbalance master, figure 6, that allows the implementation of single or multi plane unbalance by using small metallic locknuts. The CHRA integrates a semi-floating bearing with antirotation pin at the mid-plane that supports the rotating group; a cross sectional view is presented on figure 7. The vibration response on HSB is measured by an accelerometer.

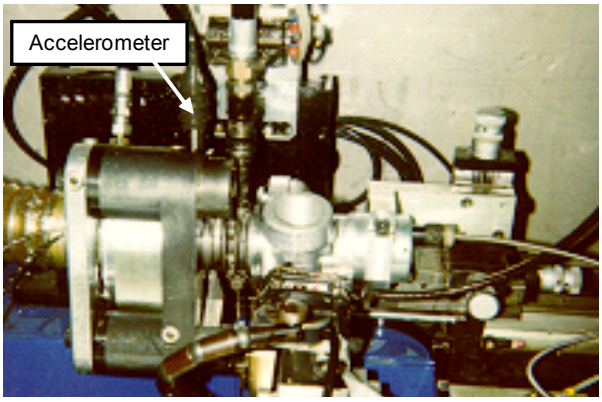

Figure 5. HIGH SPEED BALANCER

Figure 6. CHRA UNBALANCE MASTER

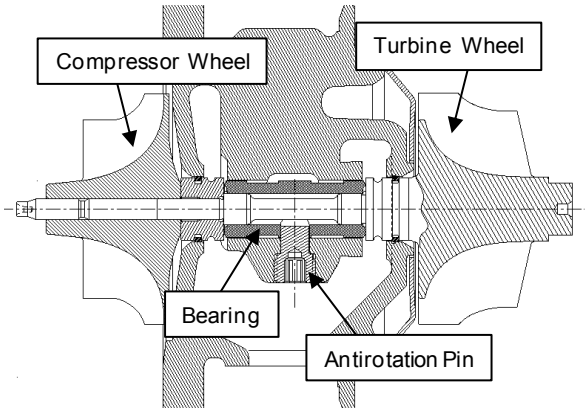

Figure 7. CROSS SECTION OF TEST CHRA

Free-free rotordynamics analysis

Figure 8 depicts the rotordynamics structural model comprising of 45 finite elements for the rotor and 4 elements for the semi-floating ring bearing. Inertia properties for the turbine, compressor and thrust collar are included at the appropriate locations. In a first step the model is validated by test data in free-free condition using the test procedure described on [25]. Figure 9 presents test/prediction data for the two first natural frequencies and associated mode shapes. The good agreement validates the rotating group structural model.

Turbocharger unbalance response and HSB synchronous vibration response

Figure 10 presents measured unbalance response on the turbine wheel nose and synchronous G level response on the high speed balancer fixture. It shows that only the first G level peak can be explained by synchronous rotordynamics analysis; it corresponds to the rotor-bearing system critical speed associated with a cylindrical deformed mode shape.

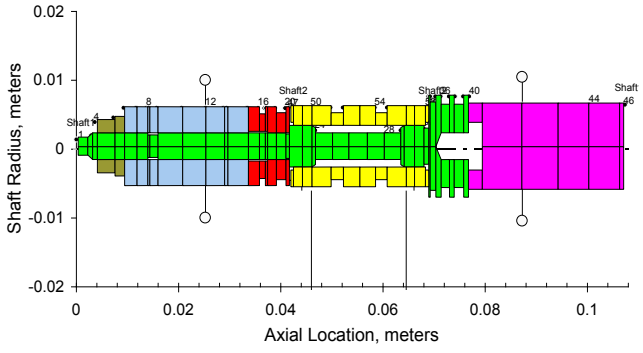

Figure 8. STRUCTURAL MODEL OF TEST TURBOCHARGER FOR ROTORDYNAMICS ANALYSIS

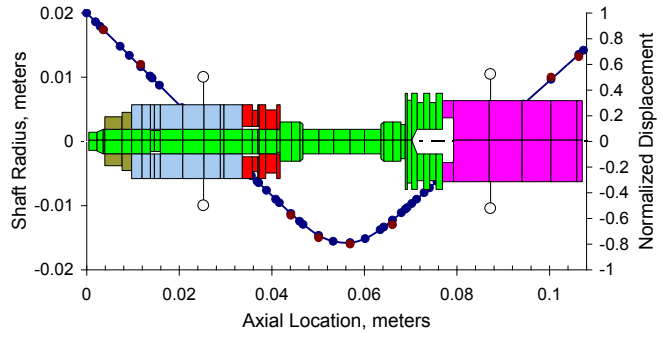

a)

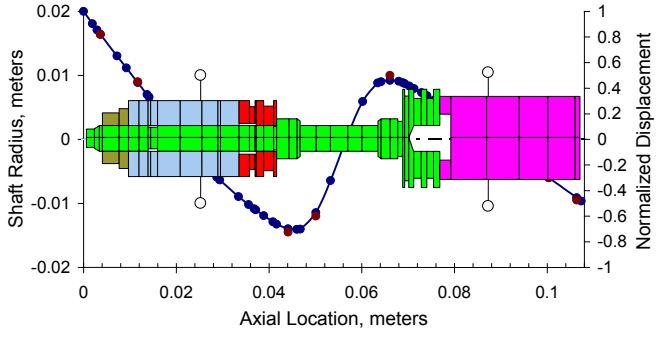

b)

Figure 9. FIRST TWO MEASURED AND PREDICTED FREE-FREE NATURAL FREQUENCIES AND ASSOCIATED MODE SHAPES OF TURBOCHARGER ROTATING GROUP

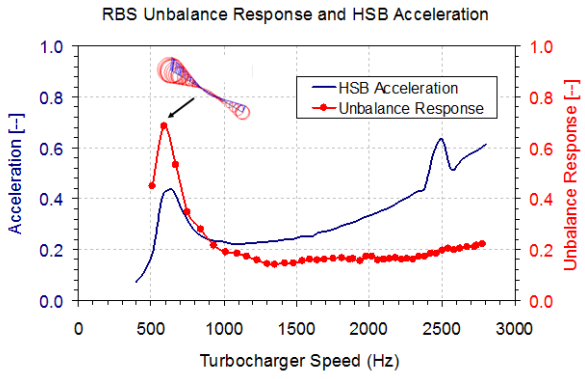

Figure 10. MEASURED CHRA MASTER UNBALANCE RESPONSE AND HSB SYNCHRONOUS G LEVEL RESPONSE

"CHRA non rotating structure - HSB fixture" dynamic behavior identification

Figure 11 shows the finite element model developed for the assembly "CHRA non rotating structure clamped on high speed balancer fixture". It features:

- Solid elements for modeling of main components (HSB fixture, nozzle, insert, centre housing) of the assembly. The chosen element is the 10-node tetrahedron, which allows automatic meshing and good correlation [26].
- Lump mass elements are added to simulate the mass of the clamping system, located at the angles of the turbine block, therefore having a cantilever effect. The local stiffness of this clamping system is ignored.
- Linear spring elements are used to simulate the vibration isolators. Their stiffness is determined from test data. Real isolators are made of elastomer material.

The finite element model is validated by a step by step experimental vibration analysis. Several FRFs are generated using a hammer for the excitation and an accelerometer for the response, figure 12. Test/prediction data presented on figure 13 shows good agreement and validates the finite element model. G level peak at 2450 Hz corresponds to a mode shape of the CHRA center housing clamped on HSB fixture, figure 14.

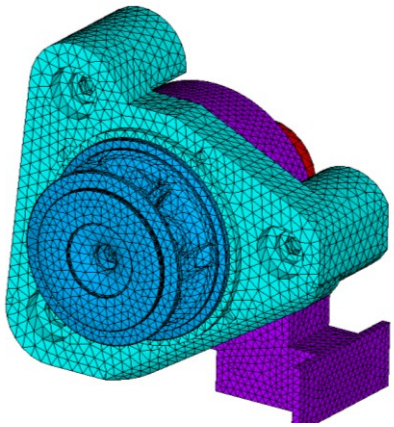

Figure 11. FINITE ELEMENT MODEL OF THE ASSEMBLY "CHRA NON ROTATING STRUCTURE-HSB FIXTURE"

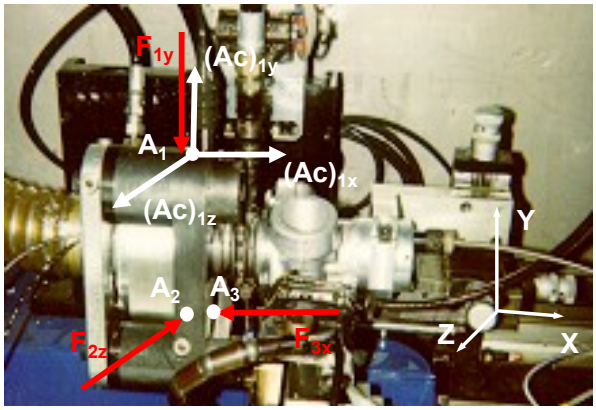

Figure 12. EXCITATION /RESPONSE POINTS ON THE ASSEMBLY "CHRA NON ROTATING STRUCTURE-HSB FIXTURE"

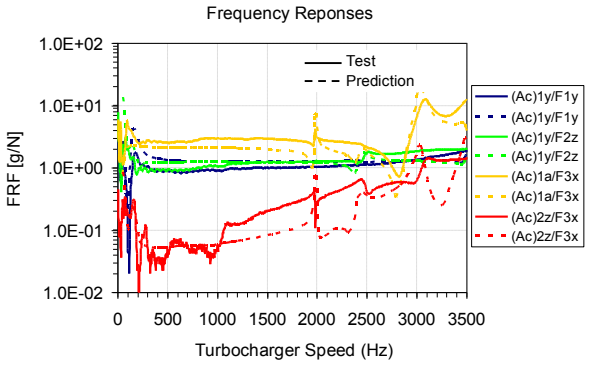

Figure 13. FREQUENCY RESPONSE FUNCTIONS OF THE ASSEMBLY "CHRA NON ROTATING STRUCTURE-HSB FIXTURE". PREDICTION AND TEST DATA

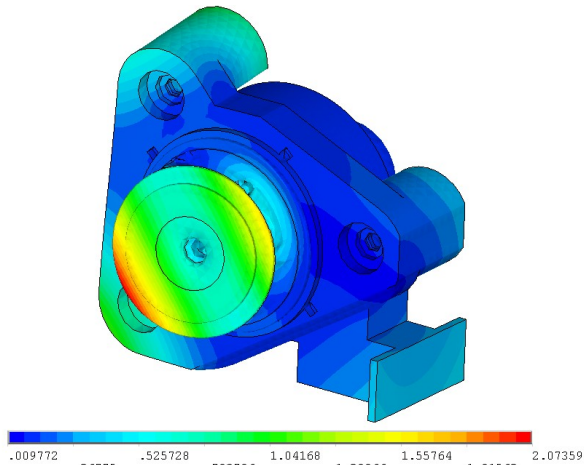

Figure 14. "CHRA NON ROTATING STRUCTURE-HSB FIXTURE" MODE SHAPE ASSOCIATED TO NATURAL FREQUENCY OF 2450 Hz

Forced synchronous vibration of the turbocharger master on HSB

4 (four) CHRA unbalance masters have been built respectively with ODminIDmin, ODmaxIDmin, ODmaxIDmax and ODminIDmax outer and inner bearing clearances. Several single and multi plane unbalance are implemented on the CHRA masters by using small locknuts. They have been run on HSB condition with Shell Tellus 100 oil, oil inlet temperature 28°C and oil inlet pressure 4 bars, and synchronous G level response is collected. Figures 15 to 16 summarize test/prediction G level data. The excellent correlation validates the developed analytical approach.

CLOSURE

In this paper, an analytical procedure is developed for prediction of forced synchronous vibration on turbocharger housings. It includes three steps: bearing loads calculation by a

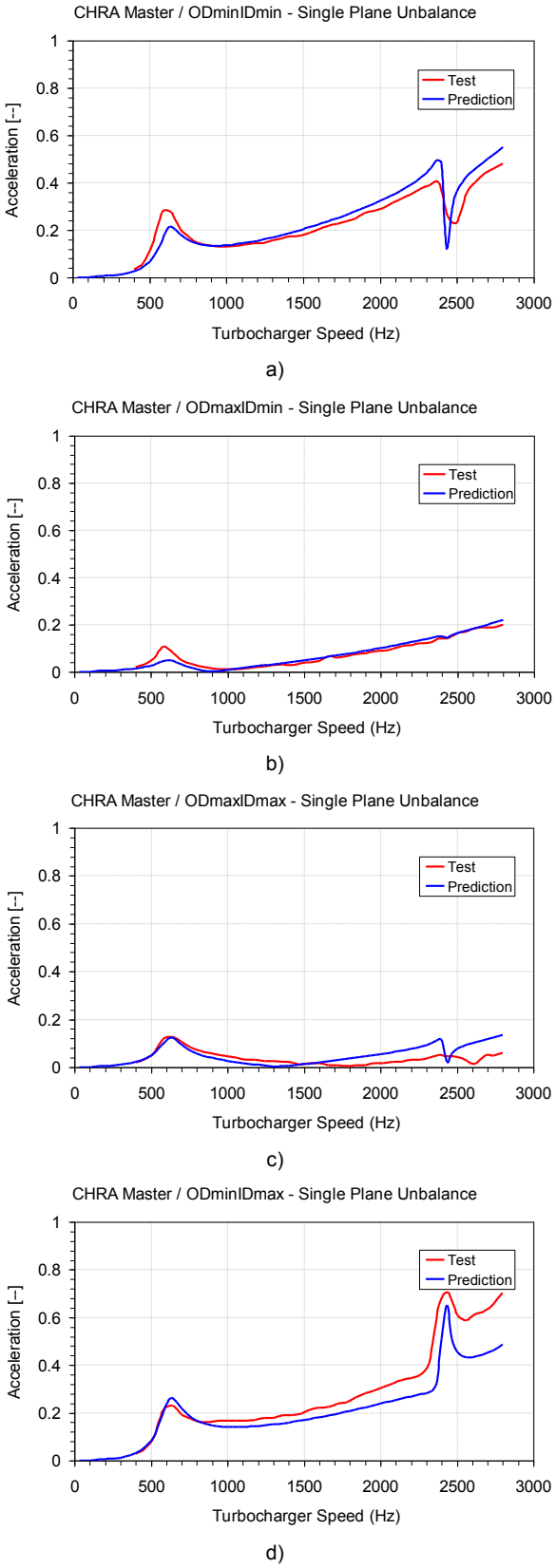

Figure 15. HSB SYNCHRONOUS G LEVEL PLOT UNDER SINGLE PLANE UNBALANCE. TEST/PREDICTION

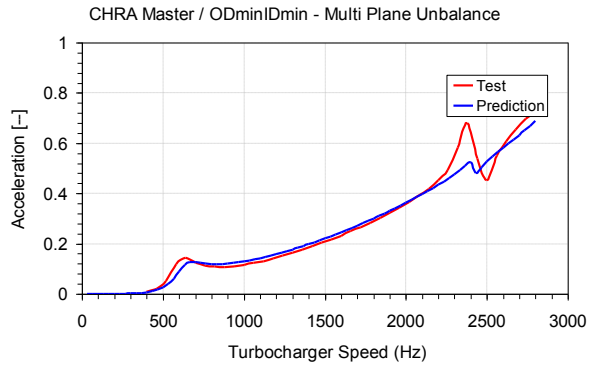

a)

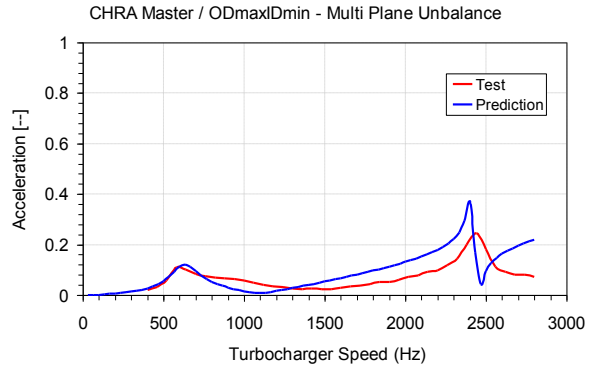

b)

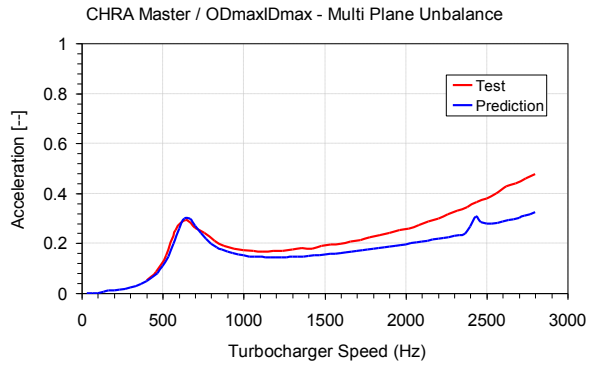

c)

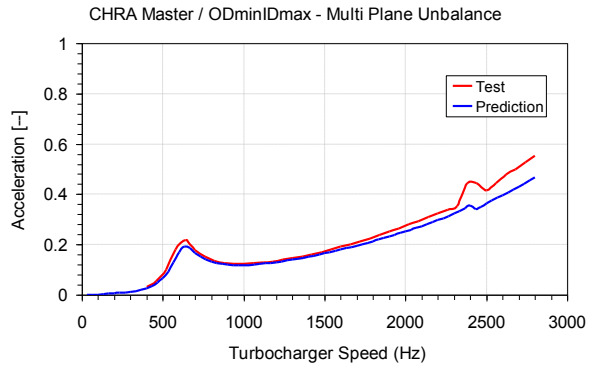

d)

Figure 16. HSB SYNCHRONOUS G LEVEL PLOT UNDER MULTI PLANE UNBALANCE. TEST/PREDICTION

rotordynamics prediction code, structural dynamics modeling of housings, and harmonic analysis that combines the first two steps for prediction of forced response on the housing structure. It is successfully validated by test data for vibration control of an automotive turbocharger on high speed balancer. This allows the development of a "product-process" approach for increased manufacturing productivity and vibration control optimization at the development stage of turbocharger.

Turbocharger subsynchronous vibration control, as well as external impact such as engine excitations, will be subject of other papers. The validated nonlinear dynamic behavior model and approach developed and presented by authors on references [27] and [28] will be updated for this purpose.

ACKNOWLEDGMENTS

The authors are indebted to Honeywell Turbo Technologies for permission to publish this work.

NOMENCLATURE

Ac,	Acceleration
B,	Bearing damping coefficient
$[C]$,	Damping matrix including shaft and bearing
c_r,	Radial bearing clearance
D,	Journal diameter
$\{d\}$,	Eigenvectors
e,	Journal eccentricity
$\{F_{ext}(\Omega t)\}$,	External synchronous excitation forces vector
F_{brg},	Bearing load
$[G]$,	Gyroscopic matrix
g,	Gravity acceleration
ID,	Inner bearing clearance
h,	Fluid film thickness
i,	Imaginary unit
K,	Bearing stiffness coefficient
$[K]$,	stiffness matrix including shaft and bearing
L,	Bearing length
$[M]$,	Mass matrix including shaft, discs and bearing inertia characteristics
m,	Mass unbalance
N_{eff},	Effective speed
N_L,	Load speed
N_J,	Journal speed
OD,	Outer bearing clearance
p,	Fluid pressure
R,	Journal radius
r,	Eigenvalues
t,	Time
U,	Journal surface speed
X, Y, Z,	Coordinate system

$\{\delta\}$, $\left\{\dot{\delta}\right\}$, $\left\{\ddot{\delta}\right\}$ Global DOF vectors (displacement, velocity and acceleration) of the system

ε, Eccentricity ratio

Φ, Phase difference between different bearings load vectors (compressor side and turbine side)

θ, Angular location

μ, Fluid viscosity

Ω, Rotational speed

ω, Imaginary part of eigenvalues

λ, Real part of eigenvalues

Λ, Load capacity number

Subscripts

brg, Bearing (bearing load)

eff, Effective (effective speed)

ext, External (external excitation force)

J, Journal (journal speed)

L, Load (load speed)

min, max, Minimum, maximum (bearing clearance)

r, Radial (radial clearance)

str, Structure (support structure)

REFERENCES

[1] Nicholas, J. C., Whalen, J. K., and Franklin, S. D., 1986, "Improving Critical Speed Calculations Using Flexible Bearing Support FRF Compliance Data", Proceedings of the 15th Turbomachinery Symposium, Texas A&M University, College Station, TX.

[2] Xu, J., and Vance, J. M., 1997, "Experimental Determination of Rotor Foundation Parameters for Improved Critical Speed Predictions", ASME Paper No. 97-GT-449.

[3] Rouch, K. E., McMains, T. H., and Stephenson, R. W., 1989, "Modeling of Rotor-Foundation Systems Using Frequency- Response Functions in a Finite Element Approach", Rotating Machinery Dynamics, **18**, pp. 157-166.

[4] Smart, M., Friswell, M. I., Lees, A. W., and Prells, U., 1998, "Estimating Turbogenerator Foundation Parameters", IMechE Journal of Mechanical Engineering Science, **212**, pp. 653-665.

[5] Wang, Q., and Maslen, E. H., 2006, "Identification of Frequency-Dependent Parameters in a Flexible Rotor System", ASME, **128**, pp. 670-676.

[6] Cherril, A. P., 1997, "Optimal Transfer Function Estimation from Frequency Response Data", Proceedings of the International Instrumentation Symposium, **43**, pp. 399-407.

[7] Cavalca, K. L., Cavalcante, P. F., and Okabe, E. P., 2005, "An Investigation on the Influence of the Supporting Structure on the Dynamics of the Rotor System", Mechanical Systems and Signal Processing, **19**, pp. 157-174.

[8] Ewins, D. J., 1984, "Modal Testing: Theory and Practice", Research Studies Press LTD., Letchworth Hertfordshire, England.

[9] Yamaguchi, T., Ogawa, M., Kasahara, T., and Arakawa, N., 1985, "Advanced Measurement Method of Frequency Response Function", Proceedings of the 3rd International Modal Analysis Conference, Orlando, Florida, Volume I, pp. 565-568.

[10] Nelson, H.D., and Meacham, W.L., 1982, "Transient Response of Rotor-Bearing Systems Using Component Mode Synthesis, Part IV Mathematical Development", Lewis Research Center Grant 3-6.

[11] Gjika, K., Groves, C., 2006, "Nonlinear Dynamic Behavior of Rotor-Bearing Systems Involving Two Hydrodynamic Films in Series: Prediction and Test. Application to High-Speed Turbochargers". Proceedings of the ASME ESDA, Paper ESDA2006-95792, Torino, Italy.

[12] Davies, P., Genin, E., Daguin, T., Marsal, D., Jeckel, D., 2010, "Down-speeding & Upgrading a Product Line for US'07 Tier2 Bin5, Eu5 & Eu6", Paper, 15. ATK Dresden, Germany.

[13] LaRue, G at al., 2006, "Turbocharger With Hydrodynamic Foil Bearings", United States Patent No: US 7,108,488 B2.

[14] Childs, D., 1993, Turbomachinery Rotordynamics, (chapter 4), D. John Wiley & Sons, Inc., NY.

[15] Nelson, H.D., 1980, "A Finite Rotating Shaft Element Using Timoshenko Beam Theory", ASME Journal of Mechanical Design, **102**, pp. 793-803.

[16] Nelson, H.D., and Meacham, H., 1981, "Transient Analysis of Rotor-Bearing System Using Component Mode Synthesis", ASME Paper No. 81-GT-10.

[17] Gjika, K., LaRue, G., 2002, "Dynamic Behavior of Rotor-Bearing Systems Involving Two Oil Films in Series: Application to High-Speed Turbocharger", Transactions of the 7th International Conference on Turbochargers and Turbocharging, IMechE, London, UK, pp. 101-115.

[18] Pinkus, O., Sternlicht, B., 1961, "Theory of Hydrodynamic Lubrication", McGraw-Hill Book Company.

[19] Stone, J. M., Underwood, A. F., 1947, "Load Carrying Capacity of Journal Bearings", SAE Quarterly Transactions, Volume 1, Number 1.

[20] Trippett, R. J., Li, D. F., 1983, "High-Speed Floating-Ring Bearing Test and Analysis", ASLE 83-AM-3E-2.

[21] Ramsey, K., 1983, "Experimental Modal Analysis, Structural Modifications and FEM Analysis on a Desktop Computer", Sound and Vibration.

[22] Gjika, K., Dufour, R., 1999, "Rigid Body and Nonlinear Mount Identification: Application to On-board Equipment with Hysteresis Suspension", Journal of Vibration and Control, **5**, pp. 75-94.

[23] Gjika, K., Dufour, R., Ferraris, G., 1996, "Transient Response of Structures on Viscoelastic and Elastoplastic

Mounts: Prediction and Experiments", Journal of Sound and Vibration, **193** (3), pp. 361-378.
[24] ANSYS, version 11.0, 2007.
[25] Gjika K., Dufour R., Swider P., Thouvenin D., 1993, "The Dynamics Behavior of a Turbocharger Rotor Involving a Subassembly", Proceedings of International Conference Structural Dynamics Modeling: Test, Analysis and Correlation, DTA & NAFEMS, Cranfield, UK, pp. 217-226.
[26] Benzley, S., Perry, E., Merkley, K., Clark, B., Sjaardama, G., 1995, "A Comparison of all Hexagonal and all Tetrahedral Finite Element Meshes for Elastic and Elasto-plastic Analysis", Proceedings of the 4th International Meshing Roundtable, Albuquerque, New Mexico, pp.179-191.
[27] Gjika, K., San Andrés, L., and LaRue, G., 2010, "Nonlinear Dynamic Behavior of Turbocharger Rotor-Bearing Systems with Hydrodynamic Oil Film and Squeeze Film Damper in Series: Prediction and Experiment", ASME J. Computational and Nonlinear Dynamics, **5**, pp. 041006.
[28] San Andrés, L., Maruyama, A., Gjika, K., and Xia, S., 2010, "Turbocharger Nonlinear Response with Engine-Induced Excitations: Predictions and Test Data", ASME J. Eng. Gas Turbines Power, **132**, pp. 032502.